

**OPEN ACCESS**

# Enhancing X-ray absorption spectroscopy with time-resolved pixel detectors

To cite this article: R.H. Menk *et al* 2026 *JINST* **21** C01039

View the [article online](#) for updates and enhancements.

## You may also like

- [About a method for compressing x-ray computed microtomography data](#)  
Lucia Mancini, George Kourousias, Fulvio Billè et al.
- [Operating synchrotron light sources with a high gain free electron laser](#)  
S Di Mitri and M Cornacchia
- [Green synthesis of gold nanoparticles: pros and cons of natural compounds](#)  
Caterina Medeot, Ahmed Alsadig, Francesco D'Amico et al.

26<sup>TH</sup> INTERNATIONAL WORKSHOP ON RADIATION IMAGING DETECTORS  
BRATISLAVA, SLOVAKIA  
6–10 JULY 2025

## Enhancing X-ray absorption spectroscopy with time-resolved pixel detectors

R.H. Menk <sup>a,b,c,\*</sup>, G. Agostini <sup>a</sup>, F. Arfelli <sup>d,b</sup>, G. Bulli <sup>d</sup>, F. Foroughi <sup>c,e</sup> and M. Li <sup>a</sup>

<sup>a</sup>Elettra Sincrotrone Trieste, Strada Statale SS14, km 163.5, 34139 Trieste, Italy

<sup>b</sup>INFN Trieste, Padriciano, 99, 34149 Trieste, Italy

<sup>c</sup>Department of Computer and Electrical Engineering, Mid Sweden University, Holmgatan 10, Sundsvall, Sweden

<sup>d</sup>Department of Physics, University of Trieste, Via A. Valerio, 2, 34127 Trieste, Italy

<sup>e</sup>Department of Physics and Engineering Physics, College of Arts and Science, University of Saskatchewan, 116 Science Place, Saskatoon, Saskatchewan, S7N 5E2, Canada

E-mail: [ralf.menk@elettra.eu](mailto:ralf.menk@elettra.eu)

**ABSTRACT.** X-ray absorption spectroscopy (XAS) is a powerful technique for probing the local atomic structure of specific elements, providing crucial insights into oxidation states and atomic coordination environments [2]. Typically performed at a synchrotron light source, XAS involves scanning the incident X-ray energy across an element's absorption edge while recording the transmitted intensity, traditionally using a set of ionization chambers [3]. This conventional approach assumes a uniform sample composition within the X-ray beam path; however, variations in thickness, structural defects, or material inhomogeneities can distort the spectra, leading to inaccurate structural parameters. In in-situ and in-operando studies, such as catalytic reactions or battery cycling, these spectral distortions significantly affect data quality. Ionization chambers provide only an averaged absorption measurement across the entire sample, potentially masking localized effects. In contrast, 2D pixel detectors enable spatially resolved absorption measurements, allowing the detection of sample heterogeneities that would otherwise go unnoticed. When combined with high frame rates, this capability becomes particularly valuable for tracking dynamic material changes under experimental conditions. In this study, we evaluate the performance of a TimePix3 hybrid pixel detector for X-ray Absorption Near Edge Structure (XANES) measurements using model and real samples at the XAS beamline at Elettra Sincrotrone Trieste [1]. Our findings demonstrate the advantages of localized detection in improving data quality and reliability, reinforcing the potential of pixel detectors as a transformative tool for complex material investigations.

**KEYWORDS:** Instrumentation for synchrotron radiation accelerators; Si microstrip and pad detectors; X-ray detectors

\*Corresponding author.



---

## Contents

<b>1</b>	<b>Introduction</b>	<b>1</b>
<b>2</b>	<b>Materials and methods</b>	<b>2</b>
2.1	Quick-XAS	2
2.2	Mock-up sample	3
2.3	Battery sample	3
<b>3</b>	<b>Results</b>	<b>4</b>
<b>4</b>	<b>Conclusions</b>	<b>6</b>

---

## 1 Introduction

The accuracy of transmission-mode X-ray absorption spectroscopy measurements strongly depends on the structural and compositional uniformity of the sample within the X-ray beam footprint. Variations in thickness, porosity, or chemical inhomogeneities can significantly distort the measured XAS spectra, leading to reduced oscillation amplitudes and erroneous structural parameters such as coordination numbers and Debye-Waller factors [4]. While meticulous sample preparation can minimize such artifacts in ex-situ experiments, in-situ conditions often introduce unavoidable changes — for instance, structural or compositional evolution in catalysts under reaction environments [5, 6, 13] or in electrode materials during electrochemical cycling [7]. Conventional ionization chambers record only the average absorption through the illuminated region, potentially masking local variations. In contrast, two-dimensional hybrid pixel detectors enable spatially resolved absorption measurements, providing a full absorption spectrum at each pixel position. Recent studies have demonstrated the power of such approaches for in-situ battery investigations, where localized charge and discharge processes can be directly visualized [8]. In this work, we present transmission-mode XAS data of a model sample and a battery sample acquired using a large, unfocused beam from a bending magnet source, to assess the data quality achievable with 2-D pixel detectors under realistic conditions. In particular, we employed the MiniPIX TPX3 detector (Advacam, Czech Republic, <https://advacam.com/camera/minipix-tpx3/>) based on the TimePix3 ASICs, offering a pixel size of  $55\ \mu\text{m} \times 55\ \mu\text{m}$  and an effective area of approximately  $1.5\ \text{cm} \times 1.5\ \text{cm}$ . The high sensitivity and wide dynamic range of the MiniPIX allowed acquisition of high-quality XAFS spectra within just a few minutes being limited by the velocity of the monochromator and not the detector. This rapid acquisition is critical for capturing real-time changes in chemical state distributions and observing reactions occurring on the microsecond scale. Before performing in situ XAFS on the battery material, the setup was validated using a mock-up sample composed of copper in different chemical states to ensure proper operation. Subsequently, the in situ two-dimensional imaging XAFS experiments were conducted on the battery sample.

## 2 Materials and methods

### 2.1 Quick-XAS

The quick XAS (QXAS) experiments were conducted at the XAFS beamline of Elettra Sincrotrone Trieste. As illustrated in figure 1, the setup followed a standard XAFS/XANES beamline configuration at a synchrotron radiation source, employing ionization chambers for transmission measurements. Additionally, the MiniPIX TPX3 detector was positioned downstream of the second ionization chamber ( $I_1$ ), allowing to acquire reference data of the same sample with the standard ionization chamber setup. The monochromator was continuously scanned across the K-absorption edge of the element of interest (Cu, 8.98 keV, energy range from 8.73 keV to 9.95 keV) for the mock-up sample and Mn (6.54 keV, from 6.33 keV to 6.73 keV) for the battery sample, while both the ionization chambers and the MiniPIX detector were read out synchronously using the AH501B quad-channel picoammeter [15] for the ionization chambers and the Pixet software for the Minipix, respectively. For all measurements discussed here the MiniPIX was operated in frame mode.

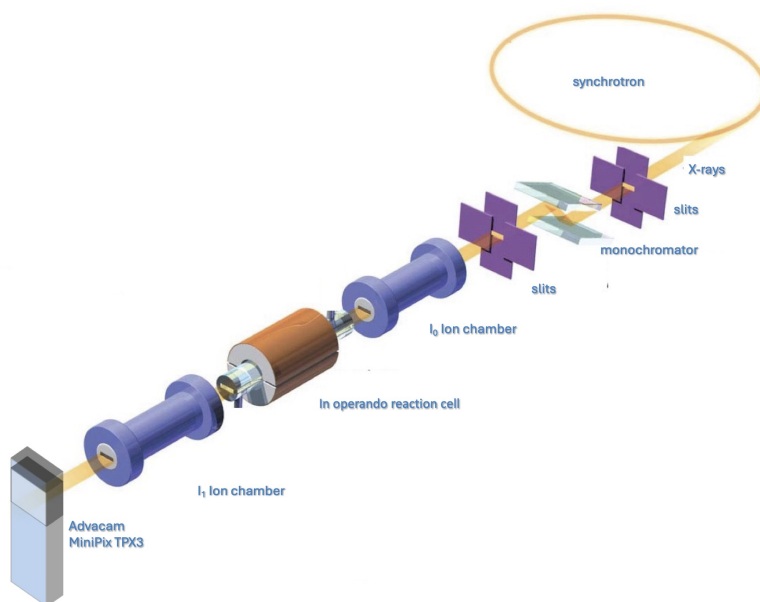


**Figure 1.** Experimental set-up as installed at the XAFS beamline of Elettra.

Typically, in both cases 2000 frames were acquired during an edge scan covering a total energy range of 397.4 eV, with an integration time of 168 ms per frame (and 0.032 s readout time), corresponding to an energy step of approximately 1.0 eV/s. This integration time was selected to ensure sufficient statistical precision, considering that the measurements were performed at a bending-magnet beamline. Since no spatially resolving  $I_0$  monitor was available, normalization was performed using two subsequent edge scans: one with the sample in place ( $I_s$ ) and one flat-field scan ( $I_f$ ) with the sample removed. The MiniPIX energy threshold was set to 4 keV, making noise-triggered photon events extremely sparse and negligible even when compared to (cosmic) charged-particle induced traces; therefore, dark-field subtraction was unnecessary. Normalized images  $N(x, y, E_i)$  were then

generated pixel by pixel at image position  $(x, y)$  for energy  $E_i$  using the negative logarithm of the ratio:

$$N(x, y, E_i) = -\log\left(\frac{I_s(x, y, E_i)}{I_f(x, y, E_i)}\right).$$

Along with the calibration and energy files, this data was input into the PyXAS [9] software for spectral fitting, followed by image segmentation.

## 2.2 Mock-up sample

The mock-up was fabricated using a two-component epoxy resin in which a pure  $Cu$  sheet (10  $\mu\text{m}$  thick Goodfellow) and  $Cu_2O$  and  $CuSO_4$  crystals were embedded. The epoxy resin was cured under overpressure to prevent bubble formation, resulting in a square pellet of 20 mm side length and 5 mm thickness (left panel of 2). The pellet then was mounted on the sample stage of the beamline (middle panel of 2) to perform the edge scan.

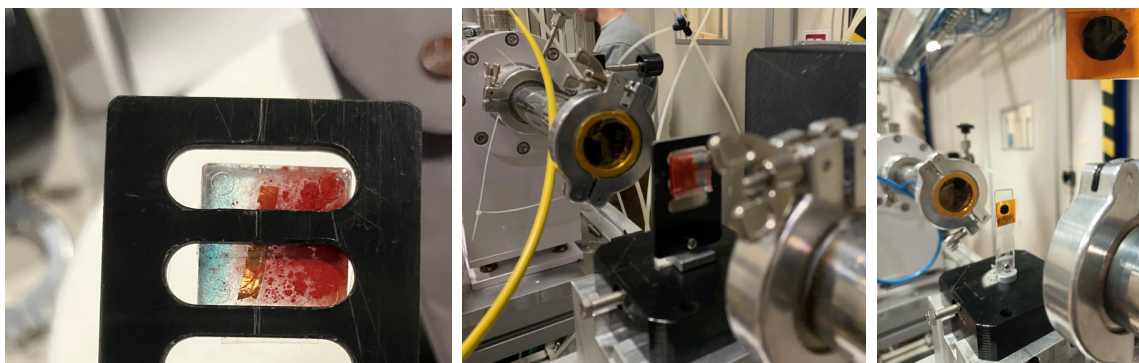


**Figure 2.** Left: photograph of the mock-up, middle: mock-up mounted on the sample stage of the XAFS beamline and right: photograph of the *ex-situ* electrode mounted on the sample stage of the XAFS beamline, inset is the image of sealed *ex-situ* electrode.

## 2.3 Battery sample

Manganese hexacyanoferrate ( $MnHCF$ ,  $Na_2Fe[Mn(CN)_6]$ ), as one of the Prussian blue analogues, has attracted wide attention as a promising cathode material for aqueous Zn-ion batteries. The synthesis of  $MnHCF$  is based on a simple and reproducible coprecipitation method, as reported in [10]. For electrode preparation, the cathode was made by mixing 70% of the as-prepared  $MnHCF$  powder, 25% Super C65 — a high-purity carbon black conductive additive — and 5% polytetrafluoroethylene. The mixture was ground until a homogeneous thin solid slice was obtained. Subsequently, an 8 mm diameter punch was used to form pellets (right panel of figure 2) with a mass loading of approximately  $5\text{--}10\text{ mg} \cdot \text{cm}^{-2}$ . The electrochemical test was conducted using a 2032-coin cell, a small, round, flat lithium primary battery with 20 mm diameter and 3.2 mm thickness: the active material was the working electrode, a zinc sheet as reference and a counter electrode in 3 moles per liter  $ZnSO_4$  aqueous electrolyte. The *ex-situ* electrodes were collected after the first charging process. The charging was conducted under a constant current of  $20\text{ mA} \cdot \text{gr}^{-1}$  with the cell potential limited between 1.0 V and 1.9 V versus  $Zn^{2+}/Zn$ .

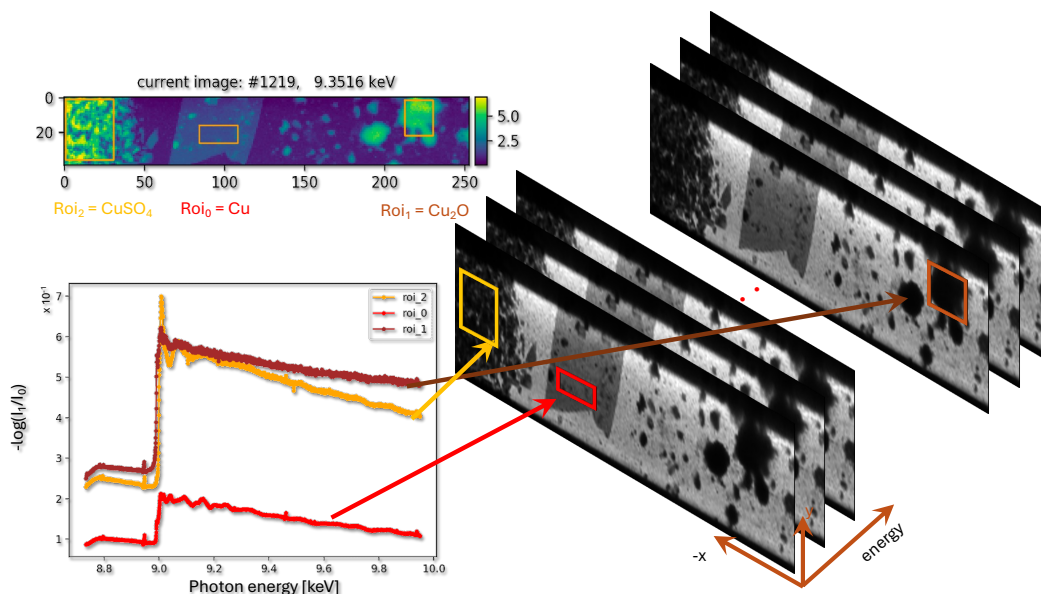


**Figure 3.** Depicted on the right hand side are some subsequent energy frames of raw data. In the upper part in the false color single frame the three different regions of interest are indicated while in the lower left hand plot the energy projections of the mean value of the ROI intensities are shown. X and Y axis scales are given in pixels.

### 3 Results

Figure 3 presents some grayscale frames of the mock-up sample acquired at a photon energy of approximately 9.352 keV, well above the Cu K-edge. The imaged area, defined by the size of the unfocused synchrotron beam, measures 14.08 mm  $\times$  2.75 mm. As shown in the false-color image, three regions of interest (ROIs) were identified, corresponding to elemental Cu (ROI<sub>0</sub>), Cu<sub>2</sub>O (ROI<sub>1</sub>), and CuSO<sub>4</sub> (ROI<sub>2</sub>), respectively. The graph in the lower-left panel displays the energy-projected intensity profiles averaged over each ROI. While variations in the edge oscillations reflect the distinct chemical states of copper present in the sample, the data exhibit the characteristic  $E^{-3.5}$  decay expected from the photoelectric effect at least far from the absorption edges.

As previously mentioned and described in [9], an additional processing step involves the removal of the pre- and post-edge slopes through linear fitting, followed by a pixel-by-pixel fitting procedure using high-fidelity calibration files corresponding to the chemical components expected in the sample. The reference spectra are shown in figure 4a, while the fitting results for the different ROIs are presented in panels b, c, and d. As illustrated in figure 4c, the excellent agreement between the fitted and experimental spectra for ROI<sub>1</sub> (Cu<sub>2</sub>O) confirms the high fitting accuracy. Somewhat less accurate fits are observed for ROI<sub>0</sub> (Cu) and ROI<sub>2</sub> (CuSO<sub>4</sub>), shown in figures 4b and 4d, however, the overall fitting quality across all ROIs is sufficient to enable reliable segmentation of the distinct chemical states.

From the fitting routines described above, oxidation-state fractions were determined for each individual image pixel, as shown in figure 5. This enables a quantitative identification of compositional variations within the sample, such as regions exhibiting slight stoichiometric differences or distinctly varying oxidation states of the same element. Furthermore, a corresponding material thickness map was generated (upper panel of figure 5) and a fitting error map (bottom panel of figure 5). In this example, the maximum fitting errors are on the order of 1–2%, which allows the reliable image segmentation of the different chemical states of Cu present in the sample.

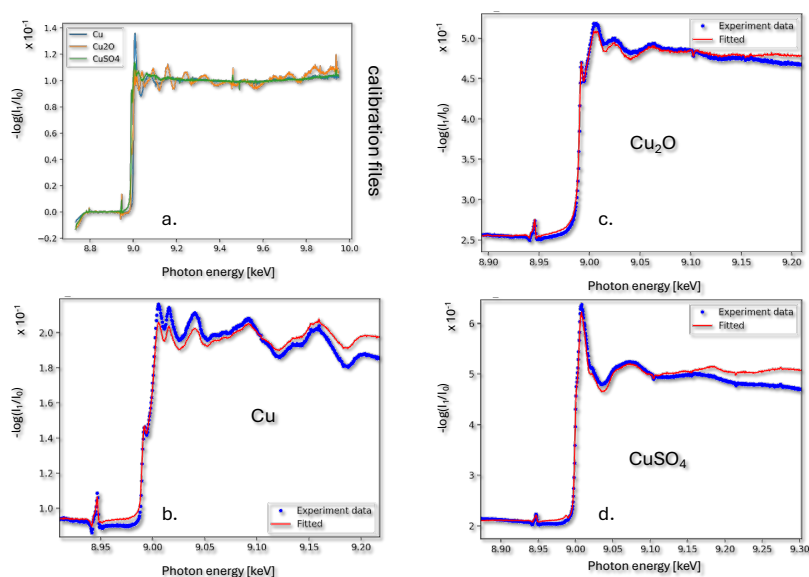


**Figure 4.** (a) Calibration files of Cu, Cu<sub>2</sub>O and CuSO<sub>4</sub>, (b)-(d) ROI fitting compared with calibration data.

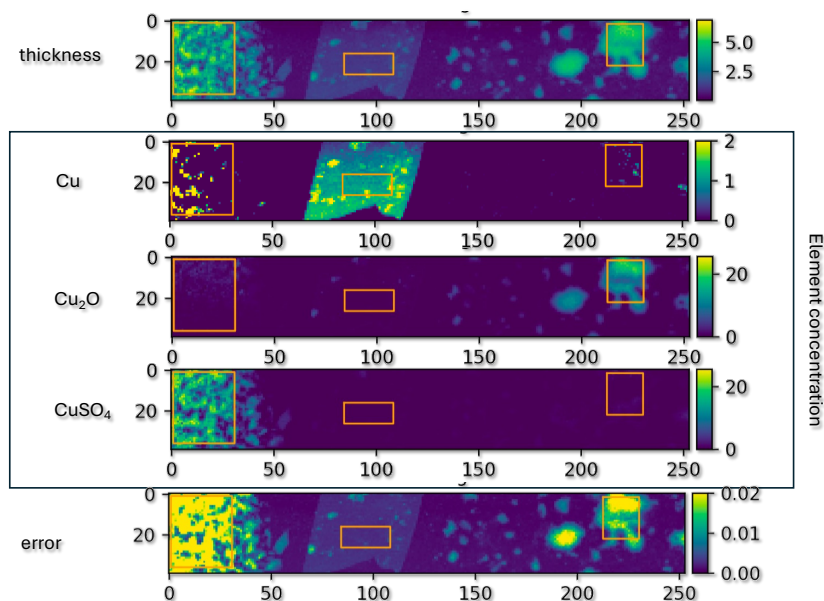


**Figure 5.** Sample thickness [mm] and decomposition of chemical state providing element concentration. X and Y axis scales are given in pixels thus  $55 \mu\text{m} \times 55 \mu\text{m}$ .

After verifying the system performance using the mock-up sample, the battery electrode was subsequently investigated. XANES measurements were first performed on the pristine electrode, confirming — as expected — the exclusive presence of Mn, as shown in figure 6a. The corresponding Mn concentration map, obtained after applying the aforementioned fitting procedures with the Mn calibration file (ref0, the Mn k-edge of MnHCF powder sample, figures 6e and 6f), exhibited a

fitting error below 0.5%, demonstrating the reliability of the procedure and indicating a homogeneous Mn distribution across the electrode.

As reported [11], in aqueous  $\text{Zn}^{2+}$  electrolyte, the MnHCF electrode suffers from fast capacity fading problem after the first charge process, due to the severe dissolution of Mn and irreversible intercalation of  $\text{Zn}^{2+}$ . Thus, a second XANES measurement was carried out for the cycled electrode, as shown in figure 6c, an uneven distribution of Mn was observed. The fitting results reveal a clear change in chemical composition of Mn, and a new  $\text{MnO}_2$  phase was observed in figure 6d, and the distribution of the new  $\text{MnO}_2$  phase quite overlapped with the Mn distribution in figure 6c. It indicates that for the remaining Mn inside the electrodes, two coordination environments were identified: Mn-O and Mn-NC, which is consistent with (extended X-ray absorption fine structure (EXAFS) fitting results reported previous [12]. The reference spectra for Mn (ref0) and the K-edge of Mn of  $\text{MnO}_2$  (ref1) are shown in figures 6e and 6f as well.

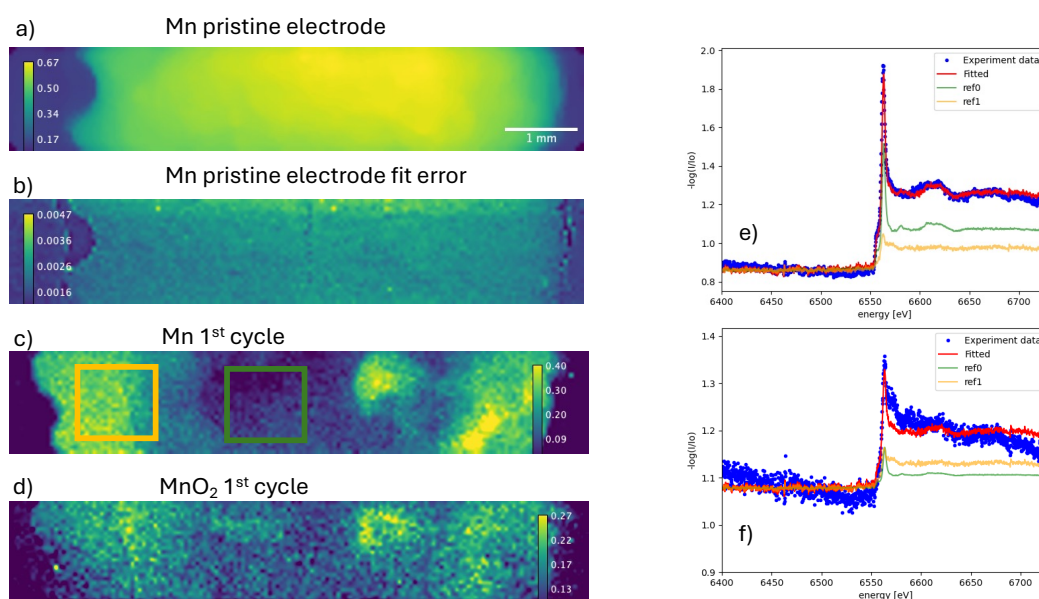


**Figure 6.** Left: Images of the pristine electrode (a) and its fit error (b). (c) and (d) depict the Mn distribution and the  $\text{MnO}_2$  distribution of chemical state after the first charging cycle.

## 4 Conclusions

The present study demonstrates the capability of hybrid pixel detectors, specifically the Timepix/Medipix family, for spatially resolved XANES and EXAFS investigations. Through the use of a mock-up sample, the system performance was first verified, showing excellent signal stability and reliable normalization despite the absence of a spatially resolving  $I_0$  monitor. The pixel-based fitting approach, implemented via the PyXAS software, enabled robust extraction of oxidation-state fractions and thickness maps with fitting errors below 2%. This allowed the identification of subtle compositional and oxidation-state variations within heterogeneous samples.

Subsequent application to an electrochemical Mn-based battery electrode further validated the technique. XANES measurements on the pristine electrode confirmed a homogeneous Mn distribution,

while post-cycling analysis revealed the formation of MnO<sub>2</sub> regions correlated with the initial Mn-rich areas. These findings illustrate the potential of 2D-resolved X-ray spectroscopic imaging for tracking chemical and structural evolution in functional materials under operating conditions.

Hybrid pixel detectors offer superior spatial resolution, single-photon sensitivity, and energy discrimination, enabling simultaneous acquisition of local XANES/EXAFS spectra across extended sample areas. Their high dynamic range and minimal dead time make them particularly suitable for time-resolved or *in-situ* studies.

In view of the existing and forthcoming fourth-generation diffraction-limited synchrotron radiation sources, which offer unprecedented brilliance and coherence, hybrid pixel detectors — whether photon-counting or high-resolution charge-integrating types [16] — will become increasingly vital for X-ray spectroscopic applications. In particular, detectors equipped with low-energy, low-gain avalanche photodiodes [17], combining high frame rates with single-photon sensitivity, are expected to play a pivotal role in exploiting the full potential of these next-generation light sources. Furthermore, event-driven readout architectures with precise time-stamping capabilities will be essential for repetitive *in-operando* experiments, enabling dynamic studies of structural and chemical transformations with high temporal and spatial resolution.

## References

- [1] A.D. Cicco et al., *Novel XAFS capabilities at ELETTRA synchrotron light source*, *J. Phys. Conf. Ser.* **190** (2009) 012043.
- [2] J.J. Rehr and A.L. Ankudinov, *Progress in the theory and interpretation of XANES*, *Coord. Chem. Rev.* **249** (2005) 131.
- [3] O. Müller, J. Stötzel, D. Lützenkirchen-Hecht and R. Frahm, *Gridded Ionization Chambers for Time Resolved X-Ray Absorption Spectroscopy*, *J. Phys. Conf. Ser.* **425** (2013) 092010.
- [4] F. Bridges, G.G. Li and X. Wang, *Monochromator-induced glitches in EXAFS data I. Test of the model for linearly tapered samples*, *Nucl. Instrum. Meth. A* **320** (1992) 548.
- [5] C.G. Schroer and J.D. Grunwaldt, *Spatially Resolved X-ray Absorption Spectroscopy*, in *In-situ Characterization of Heterogeneous Catalysts*, chapter 2, John Wiley & Sons (2013), p. 49–73 [DOI:10.1002/9781118355923.ch2].
- [6] H. Tanida et al., *In situ two-dimensional imaging quick-scanning XAFS with pixel array detector*, *J. Synchrotron Radiat.* **18** (2011) 919.
- [7] P. Müller, M. Schürmann and J. Guck, *The Theory of Diffraction Tomography*, [arXiv:1507.00466](https://arxiv.org/abs/1507.00466).
- [8] D. Lützenkirchen-Hecht et al., *XAFS data acquisition with 2D-detectors: Transmission mode XAFS and grazing incidence EXAFS spectroscopy*, *J. Phys. Conf. Ser.* **712** (2016) 012147.
- [9] M. Ge and W.-K. Lee, *PyXAS — an open-source package for 2D X-ray near-edge spectroscopy analysis*, *J. Synchrotron Radiat.* **27** (2020) 567.
- [10] M. Li et al., *Influence of Vacancies in Manganese Hexacyanoferrate Cathode for Organic Na-Ion Batteries: A Structural Perspective*, *ChemSusChem* **16** (2023) e202300201.
- [11] M. Li et al., *Electrochemical performance of manganese hexacyanoferrate cathode material in aqueous Zn-ion battery*, *Electrochimica Acta* **400** (2021) 139414.
- [12] M. Li et al., *Structural Evolution of Manganese Prussian Blue Analogue in Aqueous ZnSO<sub>4</sub> Electrolyte*, *Small* **20** (2024) 2404584.

- [13] V. Briois et al., *Hyperspectral full-field quick-EXAFS imaging at the ROCK beamline for monitoring micrometre-sized heterogeneity of functional materials under process conditions*, *J. Synchrotron Radiat.* **31** (2024) 1084.
- [14] H. Graafsma, *Requirements for and development of 2 dimensional X-ray detectors for the European X-ray Free Electron Laser in Hamburg*, *2009 JINST* **4** P12011.
- [15] <https://www.elettra.eu/technology/industry/scientific-instrumentation.html>.
- [16] A. Bergamaschi et al., *Hybrid Detectors for High Resolution Imaging*, *Microscopy Microanal.* **24** (2018) 316.
- [17] M. Andrä et al., *Development of low-energy X-ray detectors using LGAD sensors*, *J. Synchrotron Radiat.* **26** (2019) 1226.